Received: 13 November 2017 | Revised: 11 February 2018 | Accepted: 19 February 2018

DOI: 10.1002/cnm.2974

RESEARCH ARTICLE - APPLICATION

WILEY

Patient-specific simulation of guidewire deformation during transcatheter aortic valve implantation

Phuoc Vy[1,2,3,4] | Vincent Auffret[3,4,5] | Miguel Castro[3,4] | Pierre Badel[2] | Michel Rochette[1] | Pascal Haigron[3,4] | Stéphane Avril[2]

[1] ANSYS France, 69100 Villeurbanne, France

[2] Ecole Nationale Supérieure des Mines de Saint-Etienne, CIS-EMSE, INSERM: U1059, SAINBIOSE, 42023 Saint-Etienne, France

[3] INSERM, U1099, 35000 Rennes, France

[4] LTSI, Université de Rennes 1, 35000 Rennes, France

[5] CHU Rennes, Service de Cardiologie et Maladies Vasculaires, 35000 Rennes, France

Correspondence
Pascal Haigron, LTSI, Université de Rennes 1, campus de Beaulieu bat.22, 35000 Rennes, France.
Email: pascal.haigron@univ-rennes1.fr

Abstract

Transcatheter aortic valve implantation is a recent mini-invasive procedure to implant an aortic valve prosthesis. Prosthesis positioning in transcatheter aortic valve implantation appears as an important aspect for the success of the intervention. Accordingly, we developed a patient-specific finite element framework to predict the insertion of the stiff guidewire, used to position the aortic valve. We simulated the guidewire insertion for 2 patients based on their pre-operative CT scans. The model was designed to primarily predict the position and the angle of the guidewires in the aortic valve, and the results were successfully compared with intraoperative images.

The present paper describes extensively the numerical model, which was solved by using the ANSYS software with an implicit resolution scheme, as well as the stabilization techniques which were used to overcome numerical instabilities. We performed sensitivity analysis on the properties of the guidewire (curvature angle, curvature radius, and stiffness) and the conditions of insertion (insertion force and orientation). We also explored the influence of the model parameters. The accuracy of the model was quantitatively evaluated as the distance and the angle difference between the simulated guidewires and the intraoperative ones. A good agreement was obtained between the model predictions and intraoperative views available for 2 patient cases. In conclusion, we showed that the shape of the guidewire in the aortic valve was mainly determined by the geometry of the patient's aorta and by the conditions of insertion (insertion force and orientation).

1 | INTRODUCTION

Transcatheter aortic valve implantation (TAVI) is a mini-invasive procedure to replace aortic valves in the context of *aortic stenosis*. This procedure consists in delivering a fully collapsible replacement valve (*prosthesis*) onto the native aortic valve through a catheter (*sheath*). A *stiff guidewire* is first inserted in the patient's aorta with access via the femoral artery. The function of the guidewire is that of a rail along which the sheath can glide. This function is essential to ensure the navigation along the aortic arch up to the heart.

The first TAVI procedure was achieved in 2002 by Alain Cribier.[1] Since then, TAVI has permitted the treatment of patients who cannot benefit of an open heart surgery.[2,3] Nowadays, TAVI shows excellent 1-year outcomes for both

 Copyright © 2018 John Wiley & Sons, Ltd.

high-risk and intermediate-risk patients.[4] Building up on these excellent results, TAVI procedures might drastically increase in the future.

Despite this situation, a number of aspects remain to be improved, including the long-term durability and the management of possible complications. Research efforts by medical teams are focused on identifying the mechanisms of complications and determining the strategies to handle them.[5,6] It was shown that the risk of complications may be increased in case of inappropriate positioning of the delivery system in the valvular plane. For instance, paravalvular leaks,[7-9] atrioventricular block,[10] and coronary occlusion[11] could be related to the invalid implantation position of the prosthesis within the native aortic valve.

Patient-specific numerical simulations can help clinicians during preoperative planning and intraoperative navigation, as shown by different reviews recently published.[12-14] Several studies have already proved the feasibility of simulating prosthesis deployment within patient-specific anatomy. Bosmans et al validated a self-expanding prosthesis deployment model by comparing it with postoperative data. They obtained an accurate prediction of the final shape of the prosthesis.[15] Wang et al simulated balloon-expandable valve deployment within several patient-specific aortic valve geometries.[16] They illustrated how the interaction between calcifications and Valsalva sinuses could possibly induce aortic rupture. Simulation was instrumental in the decision of the medical team for the simulated patient cases. Auricchio et al suggested the measurement of the coaptation area of prosthesis leaflets to estimate the risk of transvalvular leaks.[17] Morganti et al simulated the deformed geometry of deployed prosthesis within the aortic valve.[18] They were able to predict risks of perivalvular leaks by studying the contacts between the stent and the aortic valve leaflet.

Recently, Morganti et al confirmed that the implantation depth and release angle had a crucial role on determining valve anchoring, device deformation, and risk of regurgitation.[19] This highlights the importance of correctly positioning the delivery system before and during deployment. However, the simulation of delivery tools (prosthesis, sheath, and guidewire) before deployment has not been tackled yet despite their importance on the outcome of the procedure. Such simulation raises many difficult challenges, so we focus on a single tool as a preliminary step toward this goal. To our best knowledge, the stiff guidewire used in TAVI was never simulated, despite the valuable information that can be provided on the mechanical behavior related to tool alignment. To address this issue, we introduce a novel simulation approach of the stiff guidewire in this paper. This novel simulation approach aims at predicting guidewire deformation and positioning in the first stage of TAVI procedures. The paper is organized as follows. In section 2, the mechanical problem is first formulated from a physical analysis of the stiff guidewire insertion. Then, a numerical model solving this problem is defined. Finally, the methods for our sensitivity analysis and validation are described. The simulation results are reported in section 3 and are discussed in section 4.

2 | MATERIALS AND METHODS

The purpose of the model is to predict the shape of a stiff guidewire inserted into a patient-specific aortic and ventricular geometry. The mechanical problem consists in determining the stresses and strains of a beam (the guidewire) constrained to fit within a cavity (aorta and left ventricle). The problem is solved with the finite element (FE) method by using an implicit scheme.

2.1 | Mechanical problem formulation

2.1.1 | Assumption on motions

Respiratory and cardiac movements may distort the complete structure.[20-22] However, the proposed approach was to neglect the dynamic effects of this motion on the guidewire. In addition, guidewire motion was assumed quasi-static because its low mass produced small inertial force compared with the contact forces. Only the final position of the guidewire was predicted by the final static equilibrium of the simulation.

2.1.2 | Mechanical properties

According to intraoperative observations, stiff guidewire insertion led to marginal deformations of the aorta. Thus, the aortic wall and the ventricle were assumed to remain rigid. Under this assumption, it was not necessary to model the influence of blood pressure, prestress within the vascular muscles, and the nonlinear behavior of the aortic wall over large deformations. Despite this, a model with linear elastic tissues was tested for the sake of feasibility proof.

Amplatz Super Stiff and Amplatz Extra Stiff guidewires, commonly recommended for the Corevalve™ and SAPIEN™ prostheses, respectively, were modeled in this study. The elastic properties of the Amplatz Super stiff guidewire used in CoreValve™ implantation were characterized in prior studies.[23,24] Figure 1B shows the bending stiffness along the guidewire. We did not observe any permanent deformation on the stiff guidewire caused by the intervention. Excluding gothic aortic arches, we assume that the usual curvature of the aortic arch is not sufficient to cause plastic strains.

The guidewires were designed with a straight end and may perforate the ventricular wall. To minimize the perforation risk, the guidewire has to be curved at its end before the intervention. To that purpose, clinicians manually deform the guidewire to create a curved end, as shown in Figure 1A. The obtained deformation is permanent (plastic deformation).

This predeformation of the guidewire tip was unknown for both patients considered in this study. Therefore, we investigated the impact of this predeformation through a sensitivity analysis where we varied both the angle and the radius of curvature. The straight floppy part at the end of the guidewire (Figure 1A) had a length of 40 mm. The length between the end and point C (Figure 1A) was set to 120 mm in agreement to the usual practice in the Rennes University Hospital. This corresponded to the transition between the floppy tip and the stiff body of the guidewire (Figure 1B).

2.1.3 | Contacts and boundary conditions

Interactions between the guidewire and the aortic wall result in contact forces. Friction (tangent) contact forces were neglected because the guidewire had a PTFE coating to reduce friction.

In the model, a slipping rail constrained the direction and the orientation of the proximal end (base) of the guidewire in the thoracic aorta. Translations and rotations applied by the operator were modeled as Dirichlet boundary conditions applied at the extreme distal node of the guidewire.

During actual TAVI procedures, the proximal end of the guidewire is free in the left ventricle, while the distal end is moved by the operator. Usually, during its introduction through the femoral dilator, the curved end of the guidewire can take different orientations, as shown in Figure 1C and D. Nevertheless, it remains possible to adjust the orientation when the guidewire reaches the ventricular cavity. We defined the model to take into account the possibility of different orientations in the ventricular cavity.

2.1.4 | Summary of physical parameters

The *physical parameter* input in the model is summarized in Table 1. They include the aortic geometry, the guidewire stiffness, the angle and radius of the curved tip, the axial force applied to the distal end of the guidewire, and the initial

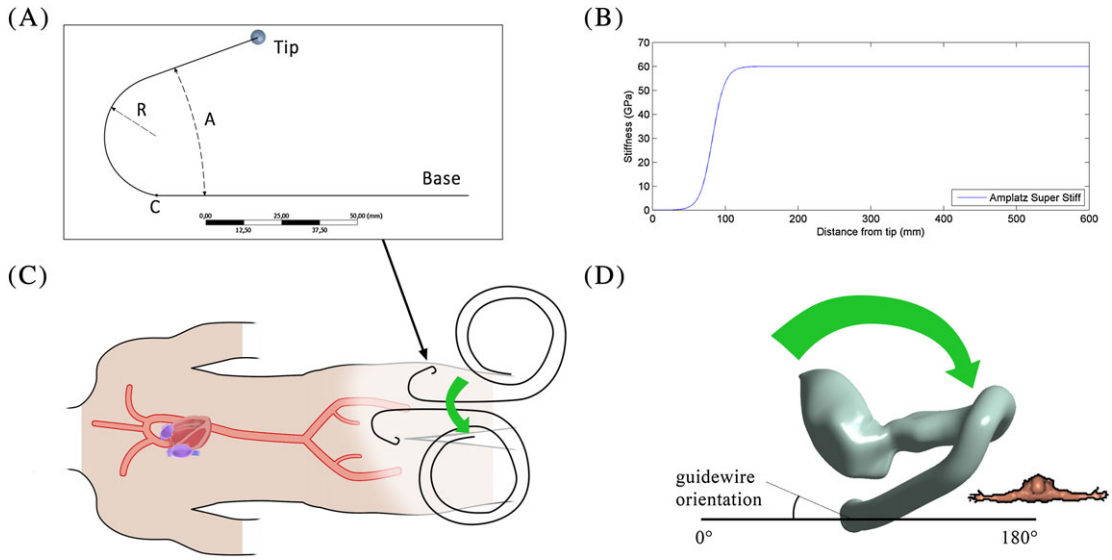

FIGURE 1 A, Model of guidewire predeformation; A, angle; R, radius of curvature; C, start of the curved shape; the tip has a rigid sphere to avoid convergence issues arising from contacts (cf. section 2.2.4). B, Stiffness profile along the guidewire based on (Luboz et al, 2011; Harrison et al, 2011). C and D, illustration of the orientation of the guidewire tip from different views

TABLE 1 Variation of parameters organized as sets of simulation, each focusing on the effect of an individual parameter

	Simulation						
Physical Parameters Focus	**1 Angle**	**2 Radius**	**3 Radius**	**4 Stiffness**	**5 Orientation**	**6 Insertion Depth**	**7-12 Numerical Param.**
Guidewire properties							
Angle (°)	20-120	20	80	20	20	20	20
Radius (mm)	30	15-30	15-30	30	25	25	30
Base stiffness (GPa)	60	60	60	20-100	60	60	60
Insertion conditions							
Force (N)	0.1-0.2	0.1-0.2	0.1-0.2	Max	0.1-0.2	Max	0.2
Orientation (°)	90	90	90	90	0-180	90	90
Initial depth (mm)	−40	−40	−40	−40	−40	7	−40

Numerical parameters Focus	**1-6 Physical param.**	**7 FKN**	**8 FTOLN**	**9 Mesh**	**10 Decay ratio**	**11 Decay/loadstep**	**12 Substep/predictor**
Contact conditions							
Stiffness coefficient (N/mm3)	1	0.1-10	1	1	0.1	0.1	1
Penetration tolerance	2	2	0.5-4	2	2	2	2
Model and solver parameters							
Mesh element size	0.4	0.7	0.7	0.4-0.7	0.7	0.7	0.7
Decay ratio	0.87	0.87	0.87	0.87	0.75-0.9	0.7-0.87	0.87
Number of loadsteps	125	125	125	125	125	50-125	125
Number of substeps	1	1	1	1	10	1	1-10
Predictor	On	Off	On	On	On	On	On/off

orientation. A sensitivity analysis was performed on these physical parameters to determine how they affect the model predictions. This analysis is designed to provide insights on the behavior of the guidewire rather than provide exact recommendation on the parameters. Indeed, those parameters are difficult to control precisely. The geometry of the stiff guidewire is approximately created as the clinician manually deforms it without any precise tool, or selected in a restricted catalog of preshaped guidewire. Likewise, the orientation of the stiff guidewire can be adjusted during its insertion but it is difficult to measure.

2.2 | Discretization and resolution method

2.2.1 | Patient-specific geometry

All patients who undergo TAVI at Rennes University Hospital provide informed consent to participate in the French National Transcatheter Aortic Valve Registry, FRANCE-TAVI,[25] allowing anonymous collection and processing of their clinical data. These interventions are commonly performed under fluoroscopic control. The 2D visualization of the aortic root can only be achieved via the injection of a contrast agent. The images used in the present study were retrospectively collected after the procedures of 2 patients who underwent TAVI at Rennes University Hospital. For both, a CoreValve prosthesis (Medtronic™) was implanted from retrograde trans-femoral access. These retrospective cases were chosen as both had intraoperative images of sufficient quality to permit their registration to the 3D preoperative CT images and to be used for the comparison with numerical simulations. The intraoperative images consisted of digitally subtracted angiography acquired during the protocol when the guidewire was inserted in the ventricle of the patient. The ascending thoracic aorta appeared clearly enough in these images, thanks to the contrast injection (Figure 2A).

A 3D preoperative CT image was routinely acquired for clinical assessment before TAVI interventions. The unsynchronized CT angioscan acquisition was performed by using Discovery CT750HD (General Electric™) (Figure 2B). A

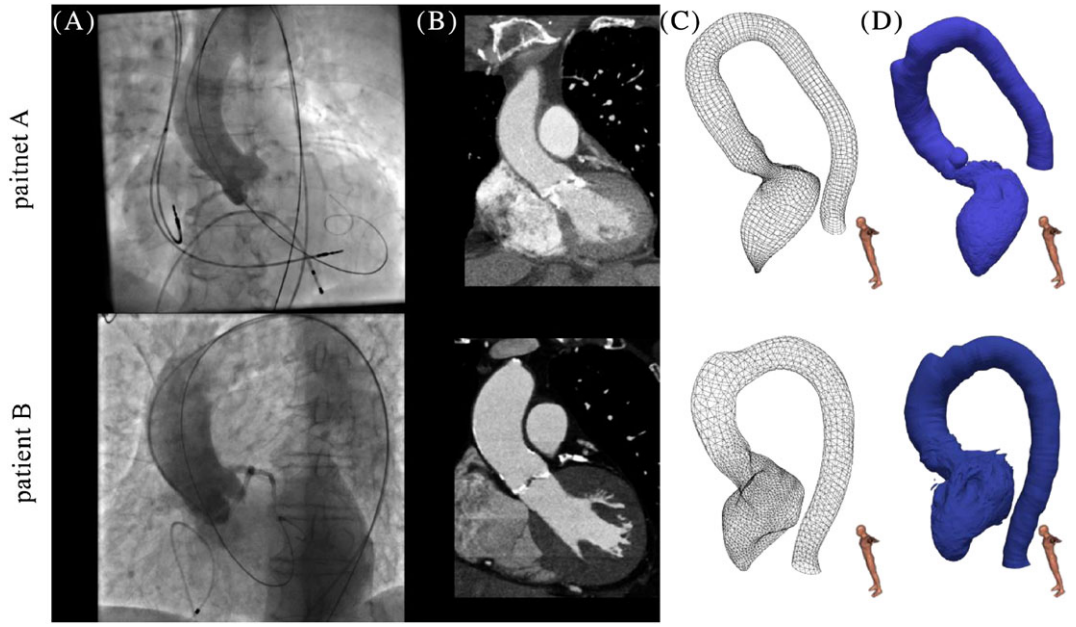

FIGURE 2 A, Intraoperative angiography of aortic root. B, Reformatted slice showing the aortic valve from preoperative CT scan. C, Finite element mesh from segmentation of CT scan. D, Segmentation from CT scan

3D reconstructed image of cardiac structures is shown in Figure 2C. In addition, the clinical protocol included a synchronized CT-scan showing exclusively the aortic valve. In our study, it was assumed that the ventricle geometry obtained in the unsynchronized CT image was fully dilated and close to diastolic state. This was verified by superimposing the synchronized and unsynchronized CT images.

Three-dimensional reconstruction of the left ventricle and aorta was interactively performed by using 3D slicer.[26] The aortic section was smoothed but did not behave well at the supra-aortic trunks (Figure 2D). Moreover, the automatic segmentation created an irregular rough surface that is unlike the real aorta or ventricle. The surface was smoothed and imported in ANSYS by using Spaceclaim, the integrated CAD module of Ansys. Only the aorta was segmented, leaving aside collateral branches and the supra-aortic trunk. The aorta was segmented from the aortic root to the distal thoracic aorta. The artifacts from the supra-aortic trunks were interactively smoothed, and a more realistic mesh was recovered (Figure 2C). This correction must be carefully performed to limit the impact on the results. We assumed that the interactions between the guidewire and the abdominal aorta, the iliac, and the femoral artery had a marginal effect on the position of the guidewire at the aortic valve because of the long sheaths specifically used in TAVI procedures.

This paper mainly focuses on the investigation of patient #1. The investigation of patient #2, reported in Appendix A, was aimed at the verification of the applicability of the model on different geometries.

2.2.2 | Meshing

The geometry was meshed in ANSYS. The rigid aorta was meshed with quadrilateral and triangle contact elements (TARGE170) as shown in Figure 1C. The default mesh had 9610 nodes for patient #1. The guidewire was meshed with quadratic 3-node beam elements based on Timoshenko beam theory (BEAM189) and line contact elements (CONTA175).

2.2.3 | Resolution scheme

Neglecting friction and plasticity, the problem was conservative. However, due to contacts and large deflections of the guidewire, it turned to be highly nonlinear. The simulations were performed on the commercial software ANSYS 17.1 with full Newton-Raphson method and sparse matrix direct solver. Time substeps ensuring convergence of the resolution were defined automatically by ANSYS. A bisection—subdivision of a substep—was performed when more than 26 equilibrium iterations were required to converge a substep. The minimum allowed time step was 5.10^{-3} s for every simulation.

2.2.4 | Boundary conditions and stabilization techniques

The resolution was achieved in 3 stages, as illustrated in Figure 3. Stage I consisted in deforming the guidewire to match the shape of the centerline of the aorta. Stage II consisted in releasing the kinematic constraints applied at stage I, leading to contact between the guidewire and the aortic wall. In stage III, the end of the guidewire could be moved (axial force or rotation) to simulate the action of an operator.

At stage II, the sudden release of the kinematic constraints is often too abrupt for the Newton Raphson algorithm to face contact nonlinearities. Hence, stabilization techniques were introduced. To this end, springs were connected to the nodes of the guidewire. Longitudinal and torsional springs were compared, with torsional springs turning out to be more successful. For each stabilized node, 3 torsional springs prevented rotations about x y, and z axes. They were defined with COMBIN14 elements. They were attached to guidewire nodes at 1 end and to a virtual anchoring node (created for that purpose) at the other end. Anchoring nodes had their displacement coupled with that of the respective guidewire nodes. Their rotations, however, were tied to the guidewire rotations with a delay of one loadstep. Torsional springs had high initial stiffness ($11.36\ \mathrm{N\ mm\ rad^{-1}}$) so that kinematic constraints could be removed without inducing sudden large displacement. The spring stiffness was decreased at each loadstep by a *decay ratio*. At the end of the stage II, all torsional springs had a null stiffness.

Two options were considered for the reaction force at the distal end of the guidewire. The first option consisted in adjusting the position of the guidewire during the whole simulation to maintain the desired reaction force. This method will be referred as *natural insertion*. Conversely, the *forced insertion* consisted in maintaining the initial depth of insertion throughout stage II.

The distal end of the guidewire was arbitrarily assigned to remain tangential to the centerline of the aorta. It happened that the actual position of guidewires observed intraoperatively at the bottom of the descending thoracic aorta may noticeably deviate from the centerline and be in contact with the wall. However, this was sufficiently far from the aortic root to induce a marginal impact on the results of this study.

Contacts were activated during stage II. Frictionless contact between patient geometry and stiff guidewire was enforced by using an augmented Lagrangian algorithm. The main parameters determining the behavior of the contact were the *contact stiffness coefficient* (FKN) and the *penetration tolerance* (FTOLN). Contact stiffness influenced the contact force applied on the bodies to prevent interpenetration. Nodes with higher penetration than the tolerance do not satisfy the contact compatibility, which is also a convergence criterion. This means that the solver has to repeat the equilibrium iteration with a higher contact force. Numerous preliminary simulations showed that direct contact between the node at the tip of the guidewire and the ventricle led to divergence of the Newton-Raphson algorithm. This issue was addressed by defining a small rigid sphere at the tip of the guidewire (cf. Figure 1A). In general, irregular contact zones such as kinks may lead to large variation of the stiffness matrix of the model which would lead to the failure of the resolution algorithm.

2.2.5 | Summary of numerical parameters

Numerical parameters are summarized in 1. They include the *mesh density*, the *number of loadsteps*, the *initial number of substeps*, the *predictor* (parameter to speed up the process of solving a substep by extrapolating better initial equilibrium iteration), the *depth of insertion*, the *decay ratio* of stabilization springs, the *contact stiffness*, and the *penetration tolerance*.

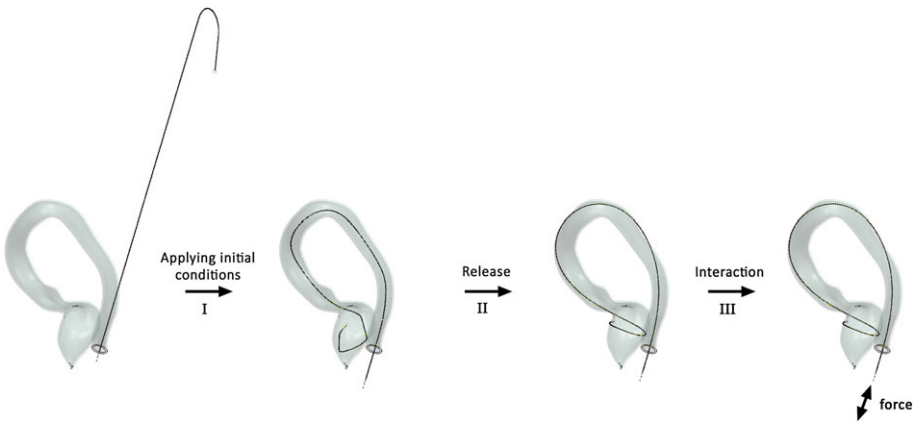

FIGURE 3 Illustration of the simulation stages. After applying initial conditions, the guidewire was constrained on the centerline. After the constraints were relaxed, the guidewire reached its final equilibrium. Then, insertion force could be varied

2.3 | Sensitivity analysis

2.3.1 | Evaluation criteria

The success of model predictions was assessed based on the following characteristics: robustness, computation time, and accuracy.

Robustness

The robustness denoted the ability of the simulation to converge in a mathematically satisfying equilibrium solution regardless of the variation of the input parameters. Convergence or divergence of the solution on a specific range of parameters was a straightforward indicator of robustness. It was observed in preliminary simulations that among all physical parameters, the axial insertion force was the main restriction for robustness (as it induced compression of the guidewire that reached its critical buckling load, which is an instability that cannot be handled with implicit resolution). Thus, maximum converging insertion force was deemed to be a relevant indicator of robustness when varying other parameters and results were presented accordingly.

Computation time

The simulations on ANSYS 17.1 were performed on a HP Z800 Workstation having 2 processors Intel® Xeon® E5620 and 12 GB of RAM. The computation time is reported as the duration of stages I and II of the simulation.

Accuracy

We defined the accuracy of the prediction as the degree of similarity between the simulation result and intraoperative data. The primary output of the simulation was the position and angle of the simulated guidewire in the aortic valve plane. The intraoperative image was a 2D fluoroscopic image, so this comparison was performed by projecting the simulation results according to the current pose of the C-arm. An example of measurement is shown in Figure 4B, where the projection of the simulation is overlapped with the intraoperative view. The aortic valve plane was manually defined according to the contour of the contrast injection. The distance between the simulation and the data was measured at the aortic valve plane in pixels (pixel size for the intraoperative data used here: 0.308 and 0.308 mm at the C-arm detector). The difference of angle was measured in degree.

A 3D/2D registration was necessary to bring the simulation results into the intraoperative coordinate system, as shown in Figure 4B. It is composed of a transformation representing the C-arm pose, a transformation positioning the preoperative CT-scan in the 3D space and a transformation corresponding to the projection performed during the generation of intraoperative images. Numerous 3D/2D registration methods can be found in the literature to obtain such transformation.[27] In this study, a rigid transform combining 3 translations and 3 rotations was iteratively defined. The

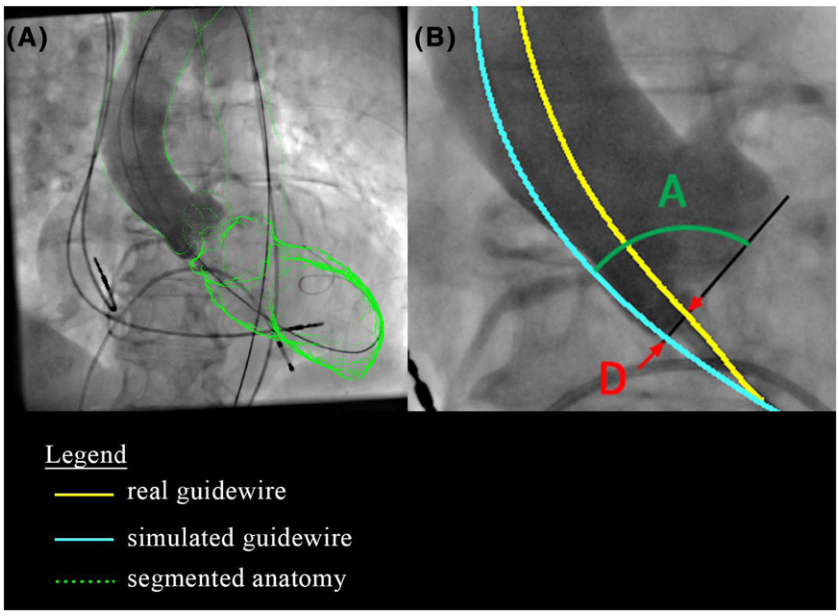

FIGURE 4 A, Projection of 3D preoperative geometry on the intraoperative 2D view according to the registration transforms. B, Intraoperative guidewire is drawn with a yellow line; simulated guidewire appear with a cyan line. The aortic valve plane is manually drawn. The distance *D* and angle *A* of the guidewires are measured at the intersection with the valve plane

C-arm pose and the intrinsic perspective projection parameters were extracted from the DICOM header of the intraoperative data to initialize the registration algorithm.

The aortic root of the 2D intraoperative image (Figure 2A) was manually contoured by an expert. The criterion for registration was the Euclidean 2D distance between the contour of the projected 3D preoperative aorta and the 2D aorta contour observed in the fluoroscopy. A distance map was computed from the 2D aortic contour with the Chamfer operator. The minimization of the distance criterion was iteratively performed by using a Powell optimization algorithm until the estimate of the 3D/2D transform was satisfactory.[28] The resulting projection is shown in Figure 4A. Two intraoperative angiographies at different pose of the C-arm were available and considered in the registration process for patient 2.

2.3.2 | Variations of input parameters

The simulations reported in Table 1 are sorted according to the variation of input parameters. Sets #1 to 6 are related to the exploration of physical parameters. Sets #7 to 12 are related to numerical parameters. The geometry of patient #1 was thoroughly studied under the 12 simulation sets.

Simulation set #1 explored the curvature angle of the guidewire tip from 20° to 120° with a 20° step at a fixed radius of curvature of 30 mm. Sets #2 and 3 explored the radius of curvature from 15 to 30 mm with a 5-mm step at a fixed angle of 20° and 80°, respectively. Set #4 explored the stiffness of the guidewire, which varied from 20 to 100 GPa. Set #5 explored the orientation from 0 to 180° with a fixed guidewire shape. Set #6 tested the forced insertion method to increase the initial depth of insertion. The guidewire was initially 47 mm deeper when using the *forced insertion* method. An insertion force of 0.1 to 0.2 N as indicated in Table 1 means that the stiff guidewire was inserted to reach a reaction force of 0.20 N and then retracted. This allowed comparing the shape of the guidewire at 0.20 and 0.10 N. Sets #4 and #6 simply had the guidewire inserted as much as possible until divergence. Finally, the model with linear elastic tissues was tested for feasibility. The tissues had an elastic modulus of 2 MPa and a Poisson's ratio of 0.49. Arbitrary boundary conditions were defined to maintain the anatomy. Elastic supports (0.15 N mm^{-3}) were defined on the thoracic aorta and the apex of the ventricle. The guidewire had a curvature of 20° and a radius of 25 mm. It was inserted with a natural insertion method to reach 0.05 and 0.1 N. The registration of the simulated deformed aorta was not performed, and accuracy evaluation was not available.

Set #7 explored the contact stiffness coefficient (FKN) from 0.1 to 10. Set #8 explored the penetration tolerance (FTOLN) from 0.5 to 4 mm. Set #9 explored the mesh density of the guidewire (1.4 node/mm, 2.5 node/mm, and 5 node/mm). The stiffness of the torsional stabilization springs was adjusted to provide the same initial level of support. Set #10 explored the decay ratio from 0.75 to 0.9.

In set #11, the decay ratio was adjusted with the number of loadsteps so that the stabilization springs reached the same stiffness at their complete deactivation across all simulations of the set (10^{-4} N mm rad^{-1}). Thus, the number of loadsteps was explored while keeping the release rate of the stabilization springs consistent. Finally, set #12 explored the relationship between the number of substep and the predictor.

3 | RESULTS

From a qualitative point of view, the model was able to converge on a large range of parameters. Table 2 reports the computation times, including minimum, maximum, and mean values, along with the diverged simulations. Table 3 reports the minimum, maximum, standard deviation, and mean values of accuracy measurements, ie, angle difference and distance rounded at the nearest pixel.

3.1 | Sensitivity to physical parameters

3.1.1 | Influence of the stiff guidewire properties

The sets investigating the effect of the curvature angle and radius (#1, #2, and #3) converged. The maximum insertion force for convergence of set #4 is reported in Table 4B. A linear regression analysis between the maximum insertion force and the stiffness of the guidewire was performed. The regression coefficient is 0.004 N/GPa, and the coefficient of determination is 0.9984.

Computation times were similar across those simulations (between 3000 and 4000 s). The simulated guidewires (#1, #2, and #3) projected on intraoperative image are shown in Figure 5B to D. The standard deviation of the angle difference and distance was low, less than 1° of angle difference and 3 px of distance. The curvature radius

TABLE 2 Computation time of simulations required to reach static equilibrium and remove all stabilization

Set	1		2		3	
Param.	Angle (°)	Computation Time (s)	Radius (mm)	Computation Time (s)	Radius (mm)	Computation Time (s)
Min	60	2,772	20	3,045	30	3,289
Max	120	3,522	30	3,521	25	4,279
Avr		3,239		3,352		3,703
Set	**4**		**5**		**6**	
Param.	**Stiffness (GPa)**	**Computation time (s)**	**Orientation (°)**	**Computation time (s)**	**Depth (mm)**	**Computation time (s)**
Min	100	3,435	0	3,081	−47	4,638
Max	20	4,707	180	3,982	7	9,572
Avr		3,835		3,401		7,105
Set	**7**		**8**		**9**	
Param.	**Contact stiffness (N/mm3)**	**Computation time (s)**	**Penetration (mm)**	**Computation time (s)**	**Mesh (node/mm)**	**Computation time (s)**
Min	3	2,846	0.5	3,521	1.4	4,056
Max	1	4,113	10	3,702	5	14,928
Avr		3,386		3,624		7,873
Set	**10**		**11**		**12**	
Param.	**Decay**	**Computation time (s)**	**Decay/loadstep**	**Computation time (s)**	**Substep/predictor**	**Computation time (s)**
Min	0.87	31,540	0.7929/75	1,821	1/on	3,521
Max	0.8	36,623	0.8402/100	2,547	10/off	14,382
Avr		33,623		2,166		7,221

Diverged simulations					
Sets	**12**		**7**	**2bis (patient 2)**	
Param.	**Substep**	**Predictor**	**FKN**	**Angle**	**Radius**
Values	10	On	0.1	20	20

of the guidewire produced the highest standard deviation. The curvature angle produced the lowest standard deviation. The projections of set #4 were not reported in the figures because the simulated guidewire shapes were too similar.

3.1.2 | Influence of the insertion conditions

Set #5 investigating the orientation converged. It required a computation time ranging from 3081 to 3982 seconds. Figure 5E shows the guidewires of set #5. The deformation of the tip is noticeably influenced by the orientation of the guidewire. The standard deviation was 2° and 4.4 px for angle difference and distance, respectively. Set #6 converged when the insertion depth was less than −18 mm or included in a range between −3.9 and 10.8 mm. Further range was not tested. The domain of convergence can be observed in the force versus displacement curve in Figure 6D. The simulated guidewires at the edge of the domain of convergence are projected in Figure 6A to C. The variation of insertion depth resulted in a large standard deviation (6.8° and 12.7 px). However, simulated guidewires from forced insertion obtained higher differences with the intraoperative guidewire. The differences produced when varying the insertion force from 0.10 to 0.20 N (natural insertion) for set #1 are reported in Table 4A. The simulated guidewires are projected

TABLE 3 Accuracy evaluation of simulation sets from the projection of simulated guidewire on intraoperative image

Set	1	Angle	2	Radius	3	Radius
Parameters	Angle Difference (°)	Distance (px)	Angle Difference (°)	Distance (px)	Angle Difference (°)	Distance (px)
Min	3.6	2	−0.5	1	−0.4	0
Max	4.4	3	−2.3	6	−1.6	5
Mean	3.9	2.3	−0.8	3.3	−0.7	2.3
Std	0.3	0.3	1.3	2.2	0.9	2.2
Set	**4**	**Stiffness**	**5**	**Orientation**	**6**	**Depth**
Parameters	**Angle difference (°)**	**Distance (px)**	**Angle difference (°)**	**Distance (px)**	**Angle difference (°)**	**Distance (px)**
Min	0	4	−0.4	3	−0.3	0
Max	0.6	5	2.8	13	−9.9	18
Mean	0.1	4.6	0.3	5.2	−5.1	9
Std	0.3	0.5	2	4.4	6.8	12.7
Set	**7**	**FKN**	**8**	**FTOLN**	**9**	**Mesh**
Parameters	**Angle difference (°)**	**Distance (px)**	**Angle difference (°)**	**Distance (px)**	**Angle difference (°)**	**Distance (px)**
Min	0	0	0.5	2	0	1
Max	−0.4	0	1.5	2	−0.5	1
Mean	−0.3	0	1	2	−0.2	1
Std	0.2	0	0.5	0	0.3	0
Set	**10**	**Decay**	**11**	**Decay / loadstep**	**12**	**Substep/predictor**
Parameters	**Angle difference (°)**	**Distance (px)**	**Angle difference (°)**	**Distance (px)**	**Angle difference (°)**	**Distance (px)**
Min	1.4	4	1.7	4	0.7	2
Max	2.1	4	2	4	1	2
Mean	1.8	4	1.9	4	0.9	2
Std	0.3	0	0.2	0	0.2	0

in Figure 5A and B. The mean values for the angle difference increased by 3.3° and distance by 1 px with the increasing force. The standard deviations remained similar for both 0.10 and 0.20 N.

3.2 | Sensitivity to numerical parameters

We observe from Table 3 that sets #7 to #12 produce very small standard deviation (less than 0.5° and 0 px). We deduce that the variation of the numerical parameters has negligible influence on the accuracy. Instead, they show a strong influence on convergence and computation time. Excessively low contact stiffness resulted in divergence. Using predictor with a large number of substep slowed the simulation and occasionally led to divergence. The decay ratio should be adjusted so that the torsional springs are deactivated with stiffness around 10^{-4} N mm rad^{-1}. The mesh density had a negligible impact on computation time. Each set is detailed in the following paragraphs.

3.2.1 | Contact conditions

In set #7, contact stiffness coefficient of 0.1 diverged. All simulations of set #8 converged. The physical parameters were angle = 100°, radius = 30 mm, and force = 0.22 N with predictor activated. The standard deviations from both contact stiffness coefficient and penetration tolerance variation were negligible, less than 0.5° for angle difference and 0 px for distance.

TABLE 4 Detailed measurements for sets #1 and #4

(a) Comparison of Insertion Force 0.10 N and 0.20 N (Set #1)				
Set #1	**Insertion Force 0.10 N**		**Insertion Force 0.20 N**	
Angle (°)	**Angle Difference (°)**	**Distance (px)**	**Angle Difference (°)**	**Distance (px)**
20	3.6	3	0.9	2
40	3.6	2	1	1
60	3.8	2	0.9	1
80	4	3	0.5	0
100	3.9	2	0	1
120	4.4	2	0.2	1
Mean	3.9	2.3	0.6	1.0
Standard deviation	0.3	0.5	0.4	0.6

(b) Maximum force insertion appears linearly dependent on stiffness of the guidewire (set #4)			
Set #4 Stiffness (GPa)	**Angle difference (°)**	**Distance (px)**	**Maximum force (N)**
20	0.1	5	0.08
40	0	5	0.16
60	-0.2	5	0.24
80	0.6	4	0.32
100	0.1	4	0.39
Mean	0.1	4.6	
Standard deviation	0.3	0.5	

3.2.2 | Model and solver parameter

Concerning set #9, the coarser mesh (1.4 node/mm) had the shortest total computation time (4056 s). The finer mesh (5 node/mm) had the longest computation time (14,928 s). Maximum insertion force of the finer mesh was 0.01 N above that of the coarser mesh. A large fraction of the computation time was spent to compute the last increments of insertion force. The standard deviation was negligible for both angle difference (0.3°) and distance (0 px).

The physical parameters for set #10 were angle = 20°, radius = 30 mm, and force = 0.20 N with a mesh density of 0.14 node/mm and 10 substeps per loadstep. The fastest simulation ran with a decay ratio of 0.87. During the deactivation of the stabilization springs at loadstep 124, their stiffness was near 10^{-4} N mm rad^{-1}. Lower decay ratio generated instability at each loadstep, which resulted in an increased computation time. Higher decay ratio slowed down the removal of stabilization springs. If the spring stiffness was still too high during the loadstep of complete deactivation of stabilization springs, instabilities arose and increased the computation time. The projections of set #9 appeared undistinguishable one from another. Careful inspection showed that very few pixels were positioned differently. The standard deviation was negligible for both angle difference (0.3°) and distance (0 px).

The physical parameters for set #11 were angle = 20°, radius = 25 mm, and force = 0.15 N. The best computation time was 1821 seconds (decay ratio = 0.7929, 75 loadsteps). The projections of the simulations appeared undistinguishable except small differences in the ventricle. The standard deviation was negligible for both angle difference (0.2°) and distance (0 px).

Finally, the physical parameters for set #11 were angle = 20°, radius = 30 mm, and force = 0.20 N. A simulation using predictor and 10 substeps per loadstep diverged. The use of predictor and the increase of the substep number did not seem to impact the accuracy of the prediction because the standard deviations were low (0.2° for angle difference and 0 px for distance). Predictor was beneficial if the number of substeps was set to 1. Conversely, predictor severely hindered the simulation when the number of substeps was set to 10.

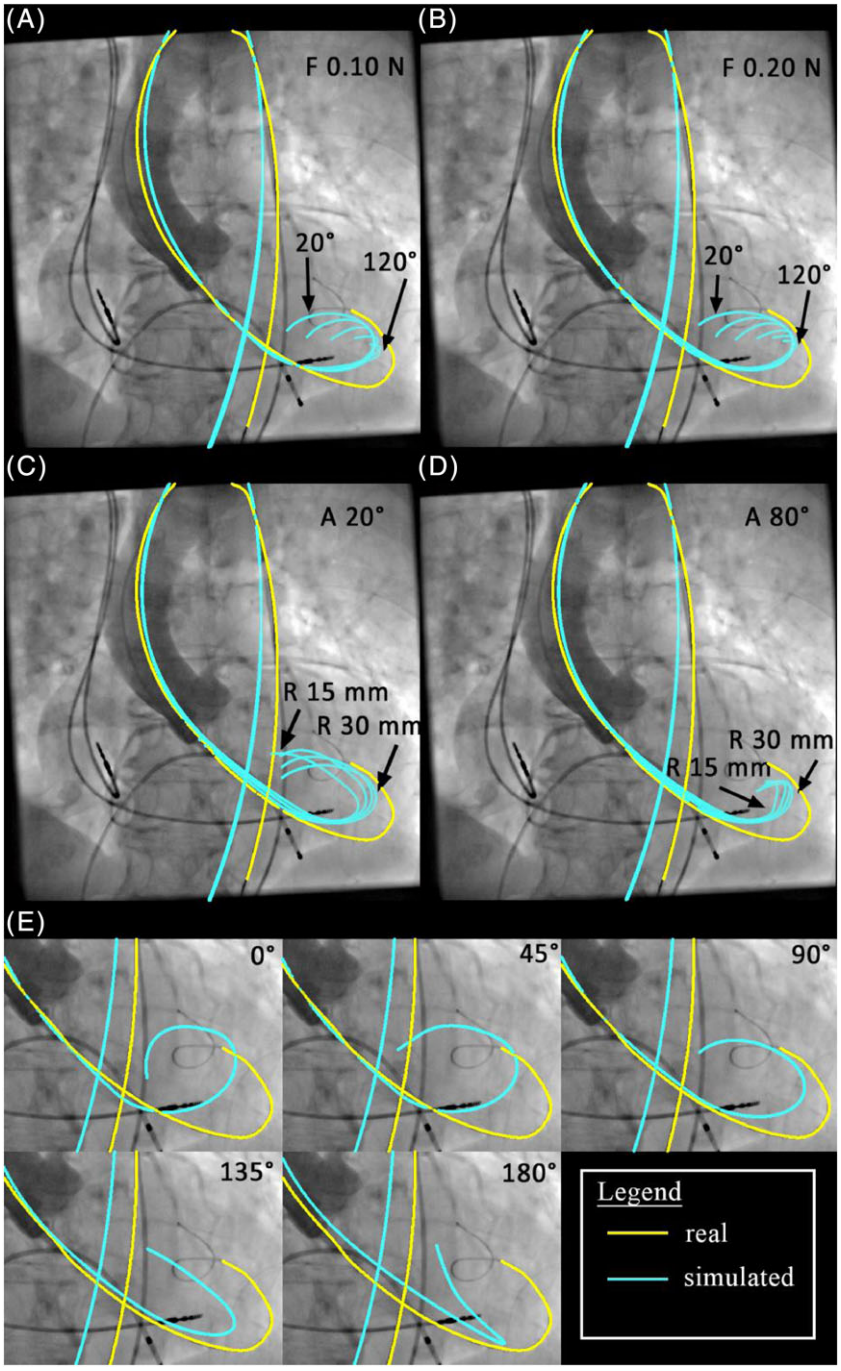

FIGURE 5 Projection of simulated guidewires. A, Set #1 exploring angle curvature at 0.10 N insertion force. B, Set #1 exploring angle curvature at 0.20 N insertion force. C, Set #2 exploring radius at 20° angle curvature. D, Set #3 exploring radius at 80° angle curvature. E, Set #5 exploring orientation

4 | DISCUSSION

4.1 | Summary

This study presented an FE modeling framework for predicting the shape of a stiff guidewire inserted into a patient-specific geometry of the left ventricle and aortic arch. The model was solved with an implicit resolution scheme in ANSYS. Then, the performance of the model was evaluated in accuracy, robustness, and speed of resolution. Nonlinearity associated with contacts proved to be a challenging problem for the implicit resolution method. Therefore, stabilization techniques were proposed to enhance the robustness of the model and overcome instabilities. The model was able to explore a wide range of parameters and provide insights on the behavior of the inserted guidewire. The results of the simulations were compared with intraoperative 2D images. Very good agreement could be obtained with respect to the intraoperative guidewire position after a thorough sensitivity analysis of the simulation problem. The guidewire properties which

a) b) c) Projections of simulated guidewires at the edges of the convergence domain reported in d). Natural insertion simulations matched closer to intra-operative data than forced insertion simulations.

d) Force-displacement graph of the insertion of guidewire. Forced insertion method allows exploring isolated domain of convergence.

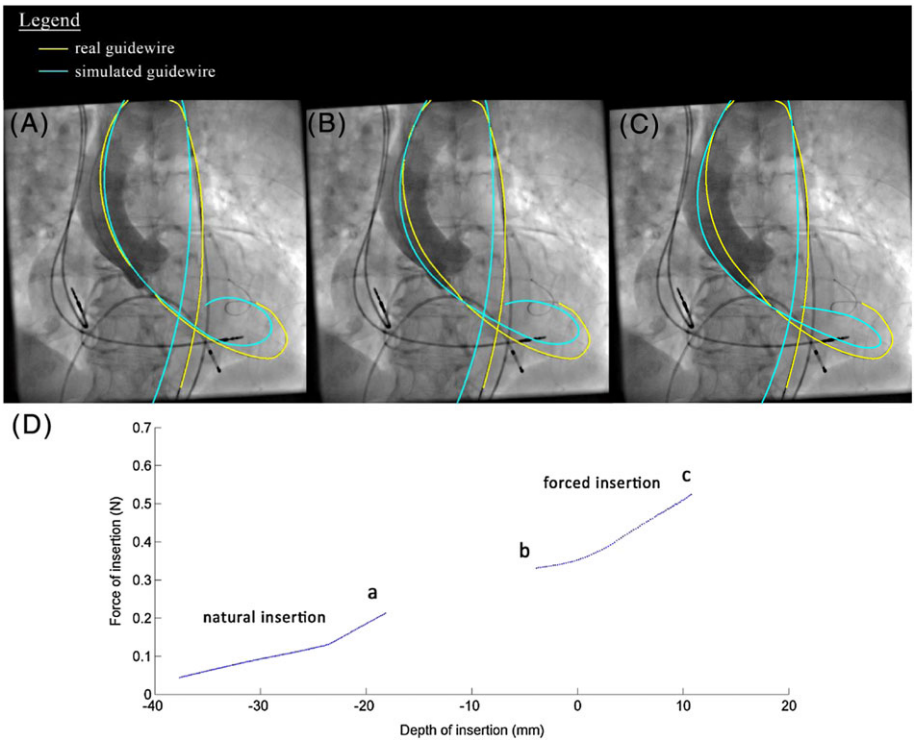

FIGURE 6 A to C, Projections of simulated guidewires at the edges of the convergence domain reported in (D). Natural insertion simulations matched closer to intraoperative data than forced insertion simulations. D, Force-displacement graph of the insertion of guidewire. Forced insertion method allows exploring isolated domain of convergence

produced the most accurate predictions were the following: curvature of 100° and curvature radius of 30 mm and insertion force of 0.20 N with a 90° orientation.

The main conclusion of the sensitivity analysis was that the patient anatomy itself mostly determined the shape of the guidewire and had a more significant impact than the guidewire curvature properties. This can be explained by the high compliance of the guidewire in its curved part compared with the straight body of the guidewire.

Excluding the patient's geometry, the influence of the physical parameters on the prediction was intricate and prevented from extracting general trends. This was especially the case for the shape of the guidewire in the left ventricle. Therefore, numerical simulations appeared to be useful to understand the insertion and navigation of endovascular tools in the aortic arch and left ventricle.

4.2 | Contribution and comparison with bibliography

Transcatheter aortic valve implantation interventions heavily rely on the experience of medical teams. Thus, numerical models can be a relevant objective complementary support. Most of the published work was focused on the numerical deployment of the prosthesis regardless of its predeployment positioning. To the best of our knowledge, no study was performed on the position of delivery tools and prosthesis at the aortic valve. Yet, it is important to deal with the position of the prosthesis because it is a concern for the success of the deployment.

Similar studies were performed by Dumenil et al and Gindre et al for the insertion of guidewires during endovascular aneurysm repair.[28,29] Other studies were dedicated to the insertion of catheter during mini-invasive treatment of cerebrovascular disease.[30-33] Among them, Lawton et al described a computationally efficient FE model based on an in-house resolution method.[34] The catheter was modeled as a thin rod, and the vessels were assumed rigid like in the present study. Schafer et al presented a method to determine the shape of the guidewire by using shortest path algorithms.[35]

Each problem was unique and raised different challenges. Cerebrovascular intervention raised challenges by navigating into a complex maze of thin arteries. Transcatheter aortic valve implantation and endovascular aneurysm repair raised more concerns on the correct placement of a prosthesis in large vessels. During TAVI, unlike other medical contexts, the guidewire is pushed against the ventricle wall. The force exerted against the guidewire; its curvature and its properties could influence its shape. Beyond the insertion of a stiff guidewire alone, it must be kept in mind that the insertion of the prosthesis and its sheath could also deform the aortic arch.

Models for cerebrovascular treatment navigation usually featured in-house implicit resolution schemes, which seemed to be successful when the vessels were rigid and little stress was generated. Conversely, models for aneurysm repair showed that explicit resolution was successful to predict the large deformations of the tools and the arteries. Likewise, simulation model for the deployment of prosthesis mainly used explicit resolution scheme so far. Despite the widespread use of explicit schemes for similar problems, we successfully used an implicit resolution scheme which is expected to provide more reliable results about stresses, strains, and contact forces.

4.3 | Interpretation of results

The main findings can be summarized as follows. Concerning the physical parameters, the results showed that the insertion force, orientation, and curvature radius strongly impacted the guidewire deformation and position at the plane of aortic valve. The curvature angle and stiffness of the guidewire had a weak influence on the inserted shape. The tests over the numerical parameters showed that they had negligible impact on the accuracy. The base of the guidewire was assumed to have little impact on the accuracy at the aortic valve, so its position was arbitrarily chosen. As such, the base of the simulated guidewire did not match the intraoperative image. The comparison of the simulation in the ventricle was not conclusive. The intraoperative ventricle appeared radio transparent so the quality of registration could not be assessed in this volume. However, all things considered, the model could reach very good accuracy in predicting the position and angle of the guidewire at the aortic valve.

Throughout the development of the model, we observed convergence difficulties for insertion force above approximately 0.20 N by using natural insertion method. A force displacement graph was plotted in Figure 6D and illustrated the domain where the simulation diverged. An analysis on the guidewire stiffness showed that the maximum insertion force was strongly correlated to the stiffness. However, the guidewire shape at the maximum insertion force was nearly identical whatever the stiffness. Using the forced insertion method, the simulation could overcome the instabilities and reach an insertion force between 0.3 and 0.5 N. However, those simulations were even more different from the intraoperative 2D image, shifting the guidewire at the aortic valve more than 10 px. Beyond 0.5 N, the simulation encountered again convergence difficulties.

The insertion of a beam against a wall might be prone to buckling effects, which can create convergence difficulties for an implicit resolution method. Euler's critical buckling load is given by the formula:

$$F = \frac{\pi 2EI}{(KL)2} \tag{1}$$

where L is the length of the beam, E is the Young's modulus of the beam (60 GPa), I is the area moment of inertia of the cross section (0.0491 mm^4), and K is the column effective length factor which was assumed to be equal to 2 as we considered one end highly constrained by contact force on the aortic wall (fixed) and the floppy tip of the guidewire free to move. Equation 1 is consistent with the correlation observed in set #4 between the stiffness of the guidewire and the maximum insertion force. To have a rough evaluation of the critical load for the guidewire, we measured that the length of the guidewire which may be subject to buckling was about 180 mm. Figure 7 shows the major contact zones on the guidewire and the measurement (in green). We obtained a critical load around 0.22 N and the proportionality coefficient relating E to F ($\pi 2I/(KL)2$) equal to 0.0037 N/GPa. This theoretical critical load was in the same range order as the maximum axial forces reached before divergence of our simulations (~0.2 N). Coincidentally, the theoretical proportionality coefficient was also in the same range as the coefficient deduced from set #4 (0.0040 N/GPa).

4.4 | Limitations

One of the main limitations of this study was related to the available data. The preoperative 3D image was unsynchronized with heart cycle, and the valve leaflets could not be extracted. The valve calcifications as seen in Figure 2B have been neglected and may impact the simulation. They could be added as rigid bodies. However, we observed that the

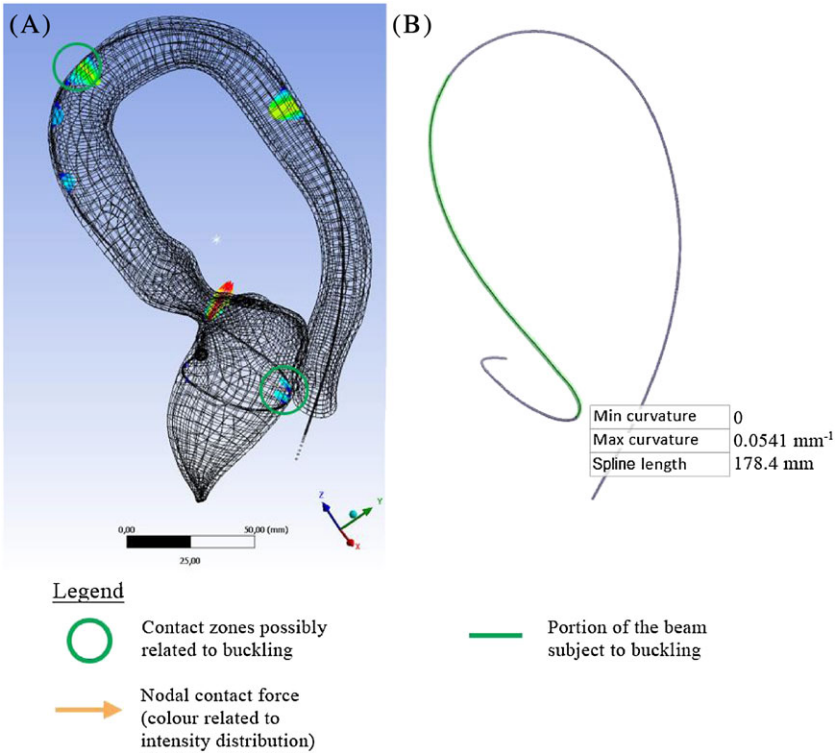

FIGURE 7 A, Contact force distribution along the simulated guidewire from set #6 (Figure 6A). The green circles highlight contact zones which may produce a buckling effect. B, Measurement of the portion of the guidewire hypothetically subjected to buckling

simulated guidewire did not touch the segmented calcifications in those patient cases specifically. The shape of the ventricle was approximate due to heartbeat effects. The creation process of the patient mesh also increased the uncertainties on the geometry of the model. The model required information on the conditions of insertion that could not be obtained from the intraoperative data, such as the inserted length of the guidewire, the insertion force, the orientation, and the shape of the curvature of the guidewire. Last, there was a possible mismatch between the model geometry and intraoperative image because of heartbeat and breathing motions. The 2D/3D registration was focused on the ascending aorta, where the contrast due to injection was highest. In the near future, the comparison of the numerical model with intraoperative images of a larger cohort of patients should provide a clearer evaluation of the reliability of the simulations and the validity of the assumptions. Finally, despite the importance of modeling the guidewire deformation, the prosthesis and the sheath should be included into the model in future studies.

The Timoshenko beam formulation was not necessarily the most appropriate choice due to the occurrence of shear-locking in field-inconsistent elements. The effect of shear-locking on accuracy and robustness was mitigated by the use of 3-node quadratic element but certainly affected the speed of the simulation. A possible direction for future works would be the improvement of the performances by including new element formulations.

4.5 | Application perspectives

The simulation framework offered interesting insights on the behavior of the guidewire and provided data to improve TAVI simulation outcomes accuracy. The framework is currently not at the stage where it can provide strategies to completely correct misalignment of the prosthesis at the aortic valve but tries to contribute toward this goal.

The prosthesis alignment is greatly determined by the sheath in comparison with the guidewire. The latter still contributes to both the alignment and the stability of the prosthesis. In exceptional cases, this small contribution is enough to allow experienced clinicians improving the alignment of self-expandable prosthesis by manipulating the guidewire. The insights provided by this simulation framework could be applied to predict whether this kind of maneuver is feasible or beneficial for a given patient anatomy and a given guidewire curvature.

In addition, the handling of the guidewire carries a risk of ventricle damage. The simulation framework could help studying the behavior of the contact between the guidewire and the ventricle to help choosing the guidewire curvature associated with the best stability and the safest distribution of contact forces on the ventricular wall. Currently, there is no general agreement regarding guidewire curvature. Increasingly more clinicians use preshaped guidewire (SAFARI™), and some center systematically use the smallest size for simplicity. Some clinicians report that small-sized preshape is

prone to unwanted migration within the ventricle and provides less stability to the prosthesis deployment. The current simulation framework has only been assessed for geometrical parameters at the aortic valve. Future works could be directed toward the improvement of prediction in the ventricle.

Finally, the centerline of the aortic valve is the starting point to visualize the prosthesis deployment. The simulated guidewire is a possible improvement to help the clinicians guess more accurately the alignment of the prosthesis in the preoperative planning stages and approach more cautiously anatomies which produce severe misalignment and have higher risks of complication. As the model matures, sheath and prosthesis may be included to help the clinician making more accurate predictions. Retrograde trans-femoral access is associated with the highest survival rate, but there could be exceptional patient cases where other accesses provide safer positioning of the prosthesis. Future works could also compare the impact of vascular accesses on prosthesis positioning.

5 | CONCLUSION

This paper presented a unique simulation framework to predict the angle and the position of a stiff guidewire in the aortic valve. The accuracy of the model was evaluated with patient intraoperative data, and good agreement could be reached. The sensitivity analysis concluded that the shape of the guidewire was mainly determined by the patient geometry and the insertion conditions. The unique use of implicit resolution scheme in this particular context required stabilization techniques to guarantee convergence. However, divergence still occurred when the guidewire was subject to buckling. A larger number of patient cases will be simulated in the future to ascertain the reliability of this method.

ACKNOWLEDGEMENTS

This work was partly supported by the French ANR within the Investissements d'Avenir program (Labex CAMI) under reference ANR-11-LABX-0004. This work has been partially conducted in the experimental platform TherA-Image (Rennes, France) supported by Europe FEDER.

ORCID

Phuoc Vy http://orcid.org/0000-0003-3813-7611

REFERENCES

1. Cribier A, Eltchaninoff H, Bash A, et al. Percutaneous transcatheter implantation of an aortic valve prosthesis for calcific aortic stenosis: first human case description. *Circulation*. 2002;106(24):3006-3008. https://doi.org/10.1161/01.CIR.0000047200.36165.B8
2. Smith C, Leon M. Transcatheter versus surgical aortic-valve replacement in high-risk patients. *N Engl J Med*. 2011;364(23):2187-2198. https://doi.org/10.1056/NEJMoa1109071
3. Leon MB, Smith CR, Mack M, et al. Transcatheter aortic-valve implantation for aortic stenosis in patients who cannot undergo surgery. *N Engl J Med*. 2010;363(17):1597-1607. https://doi.org/10.1056/NEJMoa1008232
4. Thourani VH, Kodali S, Makkar RR, et al. Transcatheter aortic valve replacement versus surgical valve replacement in intermediate-risk patients: a propensity score analysis. *The Lancet*. 2016;143(1):64-71. https://doi.org/10.1016/S0140-6736(16)30073-3
5. Masson JB, Kovac J, Schuler G, et al. Transcatheter aortic valve implantation. Review of the nature, management, and avoidance of procedural complications. *J Am Coll Cardiol Intv*. 2009;2(9):811-820. https://doi.org/10.1016/j.jcin.2009.07.005
6. Shannon J, Mussardo M, Latib A, et al. Recognition and management of complications during transcatheter aortic valve implantation. *Expert Rev Cardiovasc Ther*. 2011;9(7):913-926. https://doi.org/10.1586/erc.11.84
7. Généreux P, Head SJ, Hahn R, et al. Paravalvular leak after transcatheter aortic valve replacement: the new Achilles' heel? A comprehensive review of the literature. *J Am Coll Cardiol*. 2013;61(11):1125-1136.
8. Zegdi R, Ciobotaru V, Noghin M, et al. Is it reasonable to treat all calcified stenotic aortic valves with a valved stent? Results from a human anatomic study in adults. *J Am Coll Cardiol*. 2008;51(5):579-584. https://doi.org/10.1016/j.jacc.2007.10.023
9. Stähli BE, Maier W, Corti R, Lüscher TF, Jenni R, Tanner FC. Aortic regurgitation after transcatheter aortic valve implantation: mechanisms and implications. *Cardiovascular diagnosis and therapy*. 2013;3(1):15-22. https://doi.org/10.3978/j.issn.2223-3652.2013.02.01
10. Siontis GCM, Jüni P, Pilgrim T, et al. Predictors of permanent pacemaker implantation in patients with severe aortic stenosis undergoing TAVR. *J Am Coll Cardiol*. 2014;64(2):129-140. https://doi.org/10.1016/j.jacc.2014.04.033

11. Ribeiro HB, Nombela-Franco L, Urena M, et al. Coronary obstruction following transcatheter aortic valve implantation: a systematic review. *J Am Coll Cardiol Intv*. 2013;6(5):452-461.
12. Sun W, Martin C, Pham T. Computational modeling of cardiac valve function and intervention. *Annu Rev Biomed Eng*. 2014;16(1):53-76. https://doi.org/10.1146/annurev-bioeng-071813-104517
13. Tseng EE, Wisneski A, Azadani AN, Ge L. Engineering perspective on transcatheter aortic valve implantation. *Interv Cardiol*. 2013;5(1):53-70. https://doi.org/10.2217/ica.12.73
14. Vy P, Auffret V, Badel P, et al. Review of patient-specific simulations of transcatheter aortic valve implantation. *International Journal of Advances in Engineering Sciences and Applied Mathematics*. 2016;8(1):2-24. https://doi.org/10.1007/s12572-015-0139-9
15. Bosmans B, Famaey N, Verhoelst E, Bosmans J, Vander Sloten J. A validated methodology for patient specific computational modeling of self-expandable transcatheter aortic valve implantation. *J Biomech*. 2016;49(13):2824-2830. https://doi.org/10.1016/j.jbiomech.2016.06.024
16. Wang Q, Kodali S, Primiano C, Sun W. Simulations of transcatheter aortic valve implantation: implications for aortic root rupture. *Biomech Model Mechanobiol*. 2014;14(1):29-38. https://doi.org/10.1007/s10237-014-0583-7
17. Auricchio F, Conti M, Morganti S, Reali A. Simulation of transcatheter aortic valve implantation: a patient-specific finite element approach. *Comput Methods Biomech Biomed Engin*. 2014;17(12):1347-1357. https://doi.org/10.1080/10255842.2012.746676
18. Morganti S, Conti M, Aiello M, et al. Simulation of transcatheter aortic valve implantation through patient-specific finite element analysis: two clinical cases. *J Biomech*. 2014;2012(11):2547-2555. https://doi.org/10.1016/j.jbiomech.2014.06.007
19. Morganti S, Brambilla N, Petronio AS, Reali A, Bedogni F, Auricchio F. Prediction of patient-specific post-operative outcomes of TAVI procedure: the impact of the positioning strategy on valve performance. *J Biomech*. 2015;49(12):2513-2519. https://doi.org/10.1016/j.jbiomech.2015.10.048
20. Wang Y, Riederer SJ, Ehman RL. Respiratory motion of the heart: kinematics and the implications for the spatial resolution in coronary imaging. Magnetic resonance in medicine: official journal of the Society of Magnetic Resonance in Medicine/Society of Magnetic Resonance in Medicine *Magn Reson Med* 1995; 33(5):713–719. https://doi.org/10.1002/mrm.1910330517
21. Weber TF, Tetzlaff R, Rengier F, et al. Respiratory displacement of the thoracic aorta: physiological phenomenon with potential implications for thoracic endovascular repair. *Cardiovasc Intervent Radiol*. 2009;32(4):658-665. https://doi.org/10.1007/s00270-009-9553-3
22. Jurencak T, Turek J, Kietselaer BLJH, et al. MDCT evaluation of aortic root and aortic valve prior to TAVI. What is the optimal imaging time point in the cardiac cycle? *Eur Radiol*. 2015;25(7):1975-1983. https://doi.org/10.1007/s00330-015-3607-5
23. Luboz V, Zhai J, Odetoyinbo T, et al. Simulation of endovascular guidewire behaviour and experimental validation. *Comput Methods Biomech Biomed Engin*. 2011;14(6):515-520. https://doi.org/10.1080/10255842.2010.484003
24. Harrison GJ, How TV, Vallabhaneni SR, et al. Guidewire stiffness: what's in a name? *J Endovasc Ther*. 2011;18(6):797-801. https://doi.org/10.1583/11-3592.1
25. Auffret V, Lefevre T, Van Belle E, et al. Temporal trends in transcatheter aortic valve replacement in France. *J Am Coll Cardiol*. 2017;70(1):42-55. https://doi.org/10.1016/j.jacc.2017.04.053
26. Kikinis R, Pieper SD, Vosburgh KG. 3D slicer: a platform for subject-specific image analysis, visualization, and clinical support. In: Jolesz FA, ed. *Intraoperative Imaging and Image-Guided Therapy*. New York, NY: Springer New York; 2014:277-289.
27. Markelj P, Tomaževič D, Likar B, Pernuš F. A review of 3D/2D registration methods for image-guided interventions. *Med Image Anal*. 2012;16(3):642-661. https://doi.org/10.1016/j.media.2010.03.005
28. Dumenil A, Kaladji A, Castro M, et al. Finite element-based matching of pre- and intra-operative data for image-guided endovascular aneurysm repair. *IEEE Transactions on Bio-Medical Engineering*. 2012;60(c):1353-1362. https://doi.org/10.1109/TBME.2012.2235440
29. Gindre J, Bel-Brunon A, Kaladji A, et al. Finite element simulation of the insertion of guidewires during an EVAR procedure: example of a complex patient case, a first step toward patient-specific parameterized models. *International Journal for Numerical Methods in Biomedical Engineering*. 2015;20(4):n/a-n/a. https://doi.org/10.1002/cnm.2716):e02716
30. Wang YP, Chui CK, Cai YY, Mak KH. Topology supported finite element method analysis of catheted guidewire navigation in reconstructed coronary arteries. 1997; 24.
31. Lenoir J, Cotin S, Duriez C, Neumann P. Interactive physically-based simulation of catheter and guidewire. *Computers and Graphics (Pergamon)*. 2006;30(3):417-423. https://doi.org/10.1016/j.cag.2006.02.013
32. Nowinski WL, Chui CK. Simulation of interventional neuroradiology procedures. Proceedings - International Workshop on Medical Imaging and Augmented Reality, MIAR 2001 2001:87–94. https://doi.org/10.1109/MIAR.2001.930269
33. Cotin S, Duriez C, Lenoir J, Neumann P, Dawson S. New approaches to catheter navigation for interventional radiology simulation. *Lecture Notes in Computer Science (including subseries Lecture Notes in Artificial Intelligence and Lecture Notes in Bioinformatics)* 2005; 3750 LNCS(June 2017):534–542. https://doi.org/10.1007/11566489_66
34. Lawton W, Raghavan R, Ranjan SR, Viswanathan RR. Tubes in tubes: catheter navigation in blood vessels and its applications. *International Journal of Solids and Structures*. 2000;37(22):3031-3054. https://doi.org/10.1016/S0020-7683(99)00067-0

35. Schafer S, Singh V, Noël PB, Walczak AM, Xu J, Hoffmann KR. Real-time endovascular guidewire position simulation using shortest path algorithms. *Int J Comput Assist Radiol Surg*. 2009;4(6):597-608. https://doi.org/10.1007/s11548-009-0385-z

How to cite this article: Vy P, Auffret V, Castro M, et al. Patient-specific simulation of guidewire deformation during transcatheter aortic valve implantation. *Int J Numer Meth Biomed Engng*. 2018;e2974. https://doi.org/10.1002/cnm.2974

APPENDIX A

The simulation framework was tested on another patient geometry to verify its applicability. The rigid aorta of patient #2 was meshed with 10,294 contact elements (TARGE170) as seen in Figure 1C. The simulation set investigated the robustness of the model regarding the variation of the guidewire curvature radius. The radius ranged from 5 to 30 mm with a 5-mm step.

Most of the simulations converged at 0.20 N insertion force. The exception was radius 20 mm as the simulation could only reach 0.10 N. Figure A shows the projection of the simulated guidewires in 2 different incidences. The accuracy is reported in Table A.

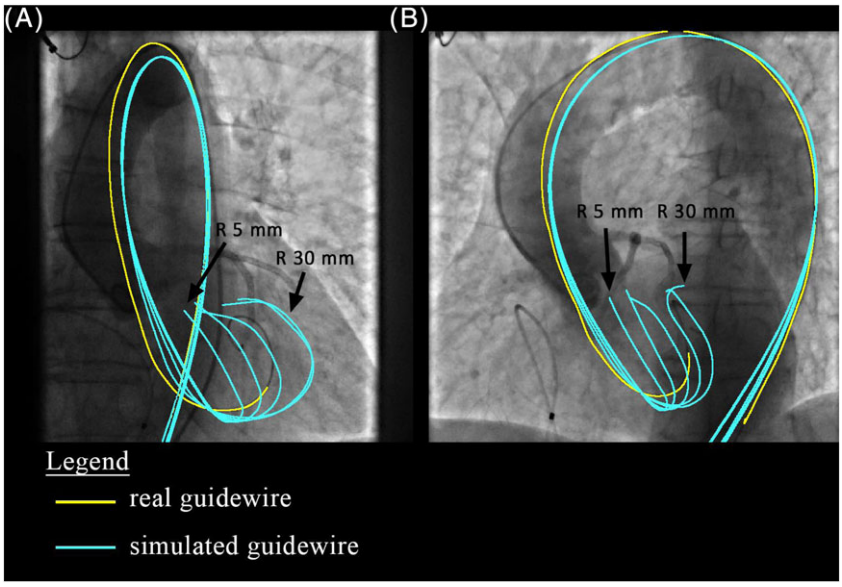

FIGURE A Superimposition of set #2bis related to the second patient case. Angle curvature was fixed at 20° and the insertion force at 0.20 N. A, Superimposition of simulated guidewires on incidence 1. B, Superimposition of simulated guidewires on incidence 2

TABLE A Test of guidewire radius for the second patient

Set #2bis Radius (mm)	Angle Difference (°)	Distance (px)	Maximum Force (N)
5	−5.2	23	0.2
10	−5.9	24	0.2
15	−5.7	23	0.2
20	−5.3	24	0.1
25	−3.4	20	0.2
30	−0.7	14	0.2
Mean	−4.4	21.3	
Standard deviation	1.5	2.9	